



## Supplementary Materials for

### **Disentangling the activity-selectivity trade-off in catalytic conversion of syngas to light olefins**

Feng Jiao *et al.*

Corresponding authors: Xiulian Pan, panxl@dicp.ac.cn; Xinhe Bao, xhbao@dicp.ac.cn

*Science* **380**, 727 (2023)  
DOI: 10.1126/science.adg2491

#### **The PDF file includes:**

Materials and Methods  
Supplementary Text  
Figs. S1 to S23  
Tables S1 to S12  
References

## Materials and Methods

### Synthesis of ZnCrO<sub>x</sub>

ZnCrO<sub>x</sub> oxide was prepared following the previously reported procedure by co-precipitation method (6, 18, 24). Briefly, 14.56 g Zn(NO<sub>3</sub>)<sub>2</sub>·6H<sub>2</sub>O, 5.6g Cr(NO<sub>3</sub>)<sub>3</sub>·9H<sub>2</sub>O and 5.25g Al(NO<sub>3</sub>)<sub>3</sub>·9H<sub>2</sub>O were dissolved in 100 mL distilled water. Subsequently, (NH<sub>4</sub>)<sub>2</sub>CO<sub>3</sub> aqueous solution was prepared as the precipitant. Co-precipitation was conducted at 70 °C. After being aged for 3 h, the precipitate was filtered and washed by distilled water, followed by drying at 110 °C and calcination at 500 °C for 1 h.

### Synthesis of SAPO-18, GeAPO-18 and MgAPO-18

GeAPO-18, SAPO-18 and MgAPO-18 were synthesized via a hydrothermal method following the same procedure as the previous report (18). Typically, aluminium isopropoxide, 85% phosphoric acid, GeO<sub>2</sub> or 30% silica sol or Mg(NO<sub>3</sub>)<sub>2</sub>, *N,N*-diisopropylethylamine (C<sub>8</sub>H<sub>19</sub>N) were dissolved in distilled water with a molar composition of Al<sub>2</sub>O<sub>3</sub>: P<sub>2</sub>O<sub>5</sub>: GeO<sub>2</sub>/SiO<sub>2</sub>/MgO: C<sub>8</sub>H<sub>19</sub>N: H<sub>2</sub>O = 0.9-1: 1: 0.04-0.07/0.02-0.05/0.04-0.11: 1.6-1.8: 42-46. The crystallization was allowed in a Teflon-lined autoclave at 160 °C for 7 days. The precipitate was washed with distilled water followed by drying overnight and calcination at 550-600 °C for 5 h. The resulting samples were denoted as MeAPO-18<sub>a</sub> with 'a' representing the mass ratio of Ge/Al, Si/Al and Mg/P.

### Synthesis of GeAPO-11 and GeAPO-5

GeAPO-11 and GeAPO-5 were synthesized via a hydrothermal method for comparison. Aluminium isopropoxide, 85% phosphoric acid, GeO<sub>2</sub>, di-*n*-propilamina (DPA) were dissolved in distilled water with a molar composition of Al<sub>2</sub>O<sub>3</sub>: P<sub>2</sub>O<sub>5</sub>: GeO<sub>2</sub>: DPA: H<sub>2</sub>O = 1: 1: 0.5: 1.4: 50. The crystallization was allowed in a Teflon-lined autoclave at 200 °C for 1 day. The precipitate was washed with distilled water followed by drying overnight and calcination at 600 °C for 5 h. The resulting samples were denoted as GeAPO-11<sub>0.026</sub>. Aluminium isopropoxide, aluminum sulfate, 85% phosphoric acid, GeO<sub>2</sub>, *N,N*-diisopropylethylamine (C<sub>8</sub>H<sub>19</sub>N) and diethylamine (DEA) were dissolved in distilled water with a molar composition of Al<sub>2</sub>O<sub>3</sub> (Al isopropoxide): Al<sub>2</sub>O<sub>3</sub> (Al sulfate): P<sub>2</sub>O<sub>5</sub>: GeO<sub>2</sub>: C<sub>8</sub>H<sub>19</sub>N: DEA: H<sub>2</sub>O = 0.6: 0.4: 1: 0.08: 0.9: 1.1: 45. The crystallization was allowed in a Teflon-lined autoclave at 160 °C for 2 days. The precipitate was washed with distilled water followed by drying overnight and calcination at 600 °C for 5 h. The resulting samples were denoted as GeAPO-5<sub>0.031</sub>. XRD and XRF results of these two zeotypes are displayed in fig. S1B and table S2. Two samples are combined with ZnCrO<sub>x</sub>, respectively, for

syngas conversion under reaction condition of 430 °C, 6 MPa, 1500 mL/(g<sub>cat</sub>·h). The results are displayed in table S12.

### Catalyst characterization

X-Ray Diffraction (XRD) patterns were obtained using a PANalytical Empyrean-100 equipped with CuK<sub>α</sub> radiation source ( $\lambda = 1.5418 \text{ \AA}$ ), operated at 40 mA and 40 kV.

The element composition of various zeotype samples were analyzed by a PANalytical Zetium X-Ray Fluorescence (XRF) spectrometer.

Water-droplet contact angle tests were conducted on the KRUSS contact angle goniometer.

Integrated differential phase contrast scanning transmission electron microscopy (iDPC-STEM) experiments were performed on the Titan Themis G3 environmental transmission electron microscope (ETEM, Thermo Scientific Company) at electron microscopy center of Dalian Institute of Chemical Physics, which worked at 300 kV with a spherical-aberration (*C*<sub>s</sub>) corrector for parallel imaging (CEOS GmbH). The microscope was aligned prior to each experiment, using a cross-grating standard sample. Specimen searching and zone axis alignment were carried out under the TEM mode. After alignment of the crystal zone axis, the microscope was switched to the STEM mode with a convergence semi-angle of 9.8 mrad to acquire iDPC-STEM images. The probe current was ~1 pA, and the dwell time is 2.5 μs/pixel. The iDPC-STEM images were acquired using a 4-quadrant DF4 detector with a high-pass filter applied on to reduce the low frequency information, and the collection angle was 2-10 mrad. Energy dispersive X-ray spectroscopy (EDS) elemental mappings over individual particles were collected using a JED-2300T, that performed on the transmission electron microscope (TEM, JEOL ARM300F). TEM worked at 300 kV with a probe spherical-aberration (*C*<sub>s</sub>) corrector.

The morphology and crystal size of the GeAPO-18 were observed by a high-resolution scanning electron microscope (SEM) using JSM-7800F from Japan Electronics Co., Ltd. Experiments were performed under high vacuum conditions with electron beam voltages ranging from 200 V to 30 kV.

X-ray absorption spectroscopy (XAS) was carried out at the BL14W beamline of Shanghai Synchrotron Radiation Facility (SSRF), which was operated at 3.5 GeV in “top-up” mode with injection current of 220 mA. EXAFS data were recorded in fluorescence mode equipped with an Electro-Lytle detector. GeO<sub>2</sub> (99.9%, Macklin) was used as a reference.

Fourier Transform Infrared Spectroscopy (FT-IR) experiment was carried out on a BRUKER INVENIO S equipped with a MCT detector. About 30.0 mg sample was pressed into a wafer (diameter 13 mm) and placed inside a quartz cell. Then it was evacuated at 450 °C for 3-4 h to obtain  $<10^{-4}$  Pa. After cooling down to room temperature, the spectra from 4000 to 1000  $\text{cm}^{-1}$  were collected by averaging 32 scans collected at 4  $\text{cm}^{-1}$  resolutions. Thereafter,  $\text{NH}_3$  adsorption was allowed at room temperature for 30 min and subsequently degassed by evacuation at 100 °C. All spectra were collected under room temperature.

Temperature-Programmed-Desorption of  $\text{NH}_3$  ( $\text{NH}_3$ -TPD) was conducted on a Micromeritics AutoChem 2920 instrument equipped with a thermal conductivity detector (TCD) detector. Typically, 100 mg sample was heated under a flowing Ar at 450 °C for 1.5 h. After cooling down to 100 °C, the sample was exposed to 5%  $\text{NH}_3/\text{He}$  for 30 min. Thereafter the sample was first swept by Ar at the same temperature for 30 min and further swept using He until a stable baseline of TCD signal was obtained. Subsequently, the TCD signal was recorded with the temperature increased from 100 to 800 °C at a heating rate of 10 °C/min.

Microcalorimetric measurements of ammonia were performed using a BT 2.15 heat flux calorimeter (Cetram, France) following previously reported procedures (18). The calorimeter was connected to a gas handling and volumetric system that employed a MKS 698A Baratron capacitance manometer for precision pressure measurement ( $\pm 1.33 \times 10^{-2}$  Pa). Before adsorption, the samples were evacuated in a quartz cell at 450 °C for 4 h. The adsorption experiments were carried out at 150 °C.

Ethylene-temperature programmed desorption (TPD) was conducted on an Intelligent Gravimetric Analyzer (IGA100, Hiden Analytical). Typically, 150 mg sample was pretreated at 300 °C in vacuum for 4 h. After cooling down to room temperature, the sample was exposed to pure  $\text{C}_2\text{H}_4$  at 1 bar for 2 h. Subsequently, the sample was swept by He for 5 h at room temperature until a stable baseline was obtained. The mass loss was recorded with the temperature increasing from RT to 300 °C at a heating rate of 5 °C/min.

The uptake rates of ethane inside zeotypes were conducted on IGA100. Typically, 30 mg zeotypes (40-60 mesh) was degassed at 300 °C for 4h and cooled down to 30 °C until a constant weight baseline. Thereafter, ethane was introduced to the chamber and the adsorption kinetics curves were recorded at 30 °C and 5 mbar. The diffusion coefficient was analyzed according to the

Fick's second law of diffusion following our previous study (22). The shape of zeotype crystal was simplified to a spherical structure model assuming the same diffusion length of 100 nm.

### Catalytic reaction

Syngas reaction was carried out in a high throughput 16-channel fixed bed reactors (Avantium Flowrence T1701) with a 2 mm inner diameter. ZnCrO<sub>x</sub> and zeotypes were mixed with a mass ratio of 2:1 and a granule size of 40-60 mesh. 5% Ar was included in the feed syngas (H<sub>2</sub>/CO = 2.5) as the internal standard for online gas chromatography (GC) analysis (Agilent 7890B). Hydrocarbons and oxygen-containing compounds were analyzed by two flame ionization detectors (FID) connected with HP-FFAP and HP-AL/S capillary columns. CO, CO<sub>2</sub>, C<sub>2</sub>H<sub>4</sub>, and Ar were analyzed by a TCD connected with Porapak Q and 5 Å molecular sieves packed columns. C<sub>2</sub>H<sub>4</sub> was taken as a reference bridge between FID and TCD.

CO conversion was calculated on a carbon atom basis, i.e.

$$\text{Conv}_{\text{CO}} = \frac{\text{CO}_{\text{inlet}} - \text{CO}_{\text{outlet}}}{\text{CO}_{\text{inlet}}} \times 100\% \quad (1)$$

Where CO<sub>inlet</sub> and CO<sub>outlet</sub> represent moles of CO at the inlet and outlet, respectively.

CO<sub>2</sub> selectivity based on C atom (Sel<sub>CO<sub>2</sub></sub>) was calculated according to:

$$\text{Sel}_{\text{CO}_2} = \frac{\text{CO}_{2\text{outlet}}}{\text{CO}_{\text{inlet}} - \text{CO}_{\text{outlet}}} \times 100\% \quad (2)$$

Where CO<sub>2outlet</sub> denotes moles of CO<sub>2</sub> at the outlet.

The selectivity of individual hydrocarbon C<sub>n</sub>H<sub>m</sub> (Sel<sub>C<sub>n</sub>H<sub>m</sub></sub>) among all hydrocarbon products based on C atom (CO<sub>2</sub> excluded) was obtained according to:

$$\text{Sel}_{\text{C}_n\text{H}_m} = \frac{n\text{C}_n\text{H}_m\text{outlet}}{\sum_1^n n\text{C}_n\text{H}_m\text{outlet}} \times 100\% \quad (3)$$

Note that the yield of light olefins was calculated by multiplying CO conversion with the selectivity of light olefins among all carbon-containing products including CO<sub>2</sub>.

To study the stability and Zn migration effect, we carried out experiment following the similar procedures as our previous study (24). First, GeAPO-18<sub>0.025</sub> granules of 20-40 mesh were physically mixed with ZnCrO<sub>x</sub> of 60-80 mesh, and subjected to syngas conversion under 430 °C, 6 MPa, 1500 mL/(g<sub>cat</sub>·h) for 100 h. After reaction, the used GeAPO-18 granules were carefully separated and characterized.

H-D exchange experiments were conducted in a fixed bed reactor with the effluents monitored by an on-line mass spectroscopy (MS). Typically, 100 mg sample was loaded in an inert

quartz tube and pretreated under a flowing Ar at 450 °C for 5 h. After cooling down to room temperature, the sample was swept using 2.5 mL/min D<sub>2</sub> and 25 mL/min 10%H<sub>2</sub>/Ar for 40 min until a stable baseline was obtained. Subsequently, the MS signals were recorded while the temperature was increased at a ramp rate of 10 °C/min.

Ethylene/H<sub>2</sub> conversion model experiments were performed in a fixed-bed stainless steel reactor equipped with a quartz lining. Typically, 250 mg sample (20-40 mesh) was diluted by 200 mg inert quartz sand. The catalyst was swept in N<sub>2</sub> from room temperature to 400 °C, then a pre-mixed gas, composed of 1.2% C<sub>2</sub>H<sub>4</sub>, 66.6% H<sub>2</sub> and 32.2% Ar, was introduced as the feed at 100-200 mL/min and the reaction was allowed at 4 MPa and 400 - 460 °C. Products were analyzed by an online GC (Shimadzu GC-2014), equipped with an FID and a TCD. To clarify the effect of CO in this model experiments, 10% CO balanced with Ar was simultaneously introduced into the reactor at a flow rate of 40 mL/min.

C<sub>2</sub>H<sub>4</sub> conversion was calculated on a carbon atom basis, i.e.

$$\text{Conv}_{C_2H_4} = \frac{C_2H_{4\text{inlet}} - C_2H_{4\text{outlet}}}{C_2H_{4\text{inlet}}} \times 100\% \quad (4)$$

Where  $C_2H_{4\text{inlet}}$  and  $C_2H_{4\text{outlet}}$  represent moles of C<sub>2</sub>H<sub>4</sub> at the inlet and outlet, respectively.

### DFT calculation

All energetics and structural relaxations were calculated using density functional theory (DFT), as implemented in the Vienna *ab initio* simulation package (VASP). In addition, the projector augmented-wave (PAW) scheme and generalized gradient approximation (GGA) method at the level of the revised Perdew–Burke–Ernzerhof (rPBE) functional were used. The convergence criteria of energy and force were set to 10<sup>-4</sup> eV and 0.05 eV·Å<sup>-1</sup> in structural optimizations. Kinetic energy cutoff was specified to 400 eV, and sampled the Brillouin zone with the  $\Gamma$  point.

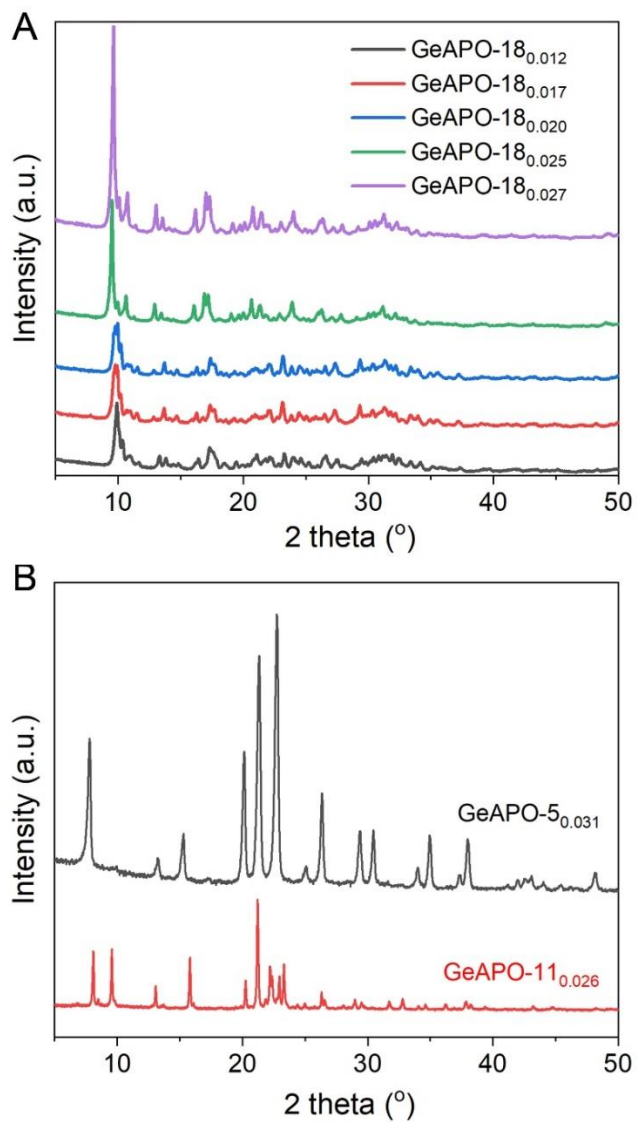
An AlPO-18 unit cell was used with a = 13.71 Å, b = 12.73 Å, c = 18.57 Å.

The adsorption energy of ammonia and ethylene is calculated as follows:

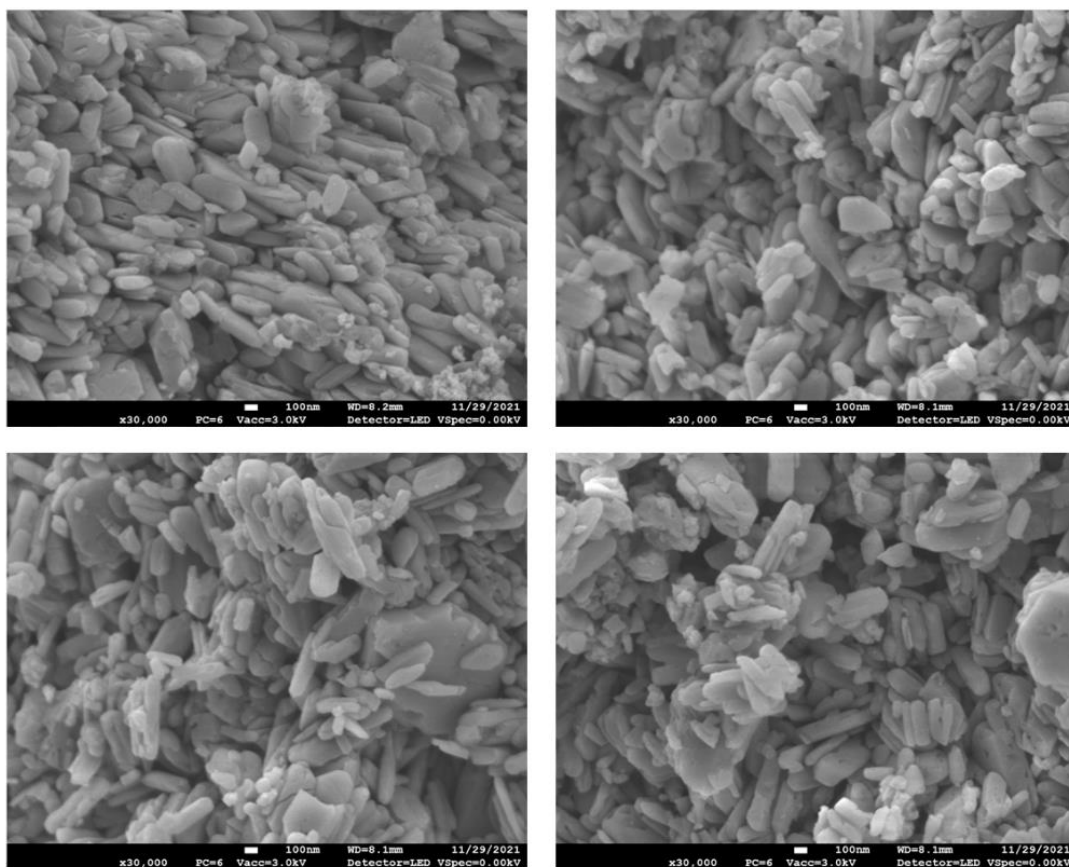
$$E_{AD-NH_3} = E_{total} - E_{ZEO} - E_{NH_3}$$

$$E_{AD-C_2H_4} = E_{total} - E_{ZEO} - E_{C_2H_4}$$

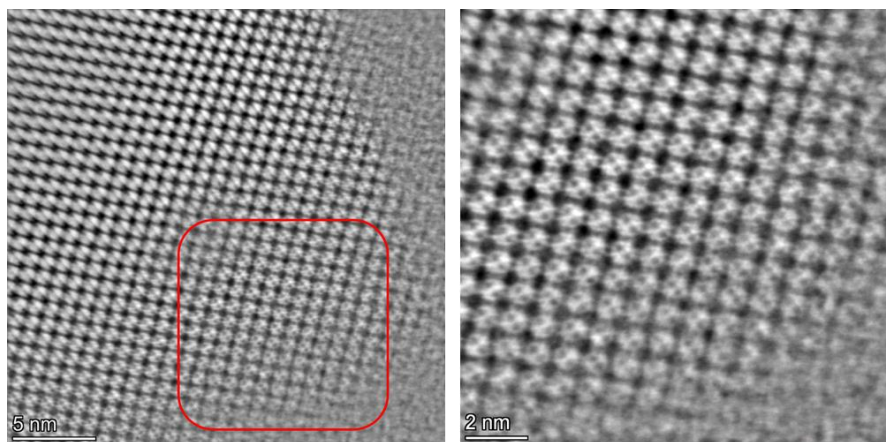
$E_{total}$  is the energy of zeolite after adsorbing gas molecules, and  $E_{ZEO}$  is the energy of individual zeolite. The adsorption models are optimized under the condition of all atoms relaxation.



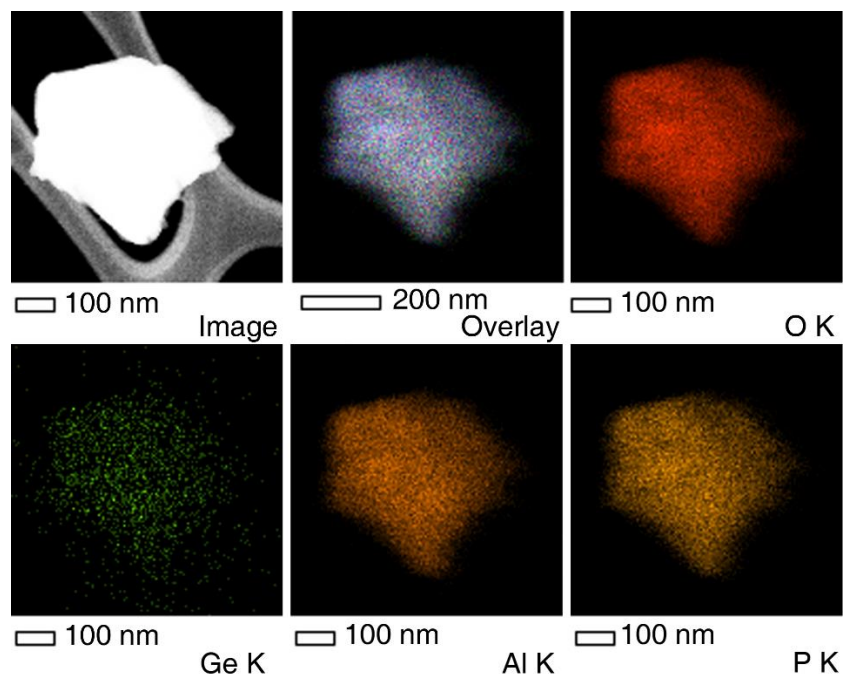
**Fig. S1. XRD patterns of (A) GeAPO-18<sub>a</sub>, (B) GeAPO-11<sub>0.026</sub> and GeAPO-5<sub>0.031</sub> with the subscript denoting the mass ratio of Ge/Al measured by XRF.**



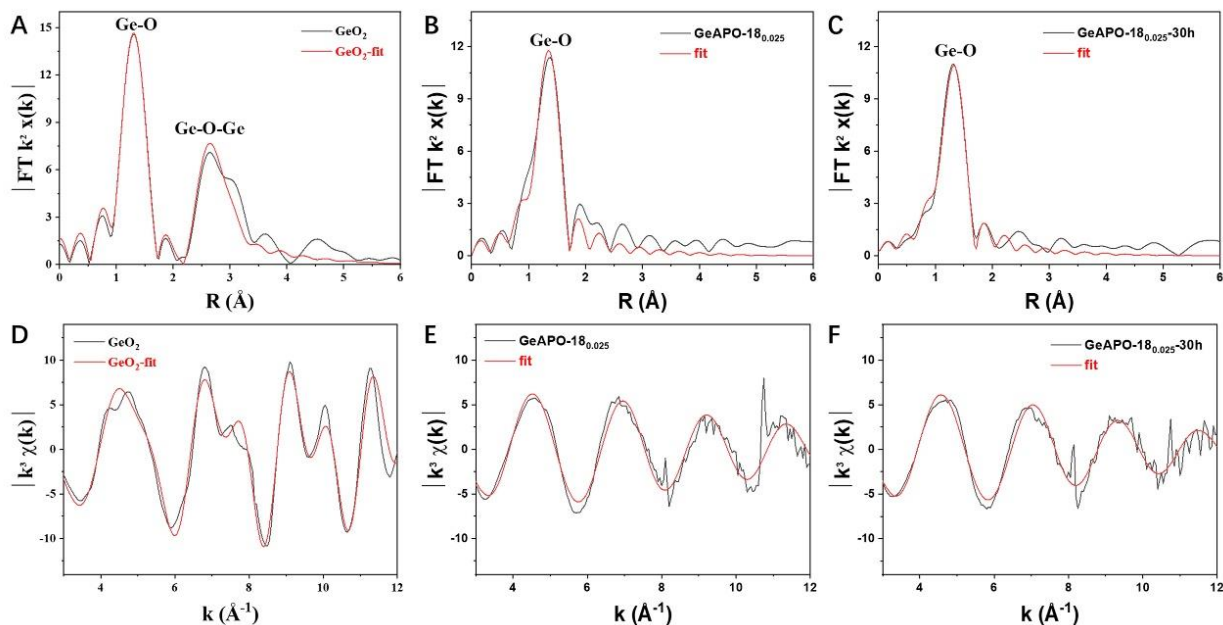
**Fig. S2. SEM images of the randomly scanned regions of GeAPO-180.025.**



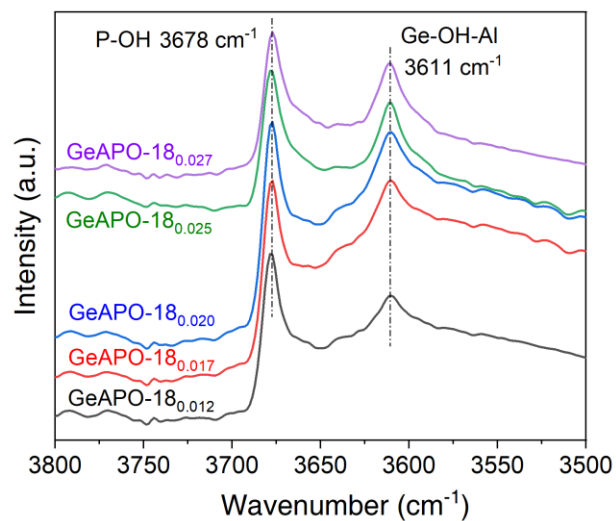
**Fig. S3. Integrated differential phase contrast scanning transmission electron microscopy (iDPC-STEM) images of GeAPO-18<sub>0.025</sub>, which shows a characteristic AEI structure.**



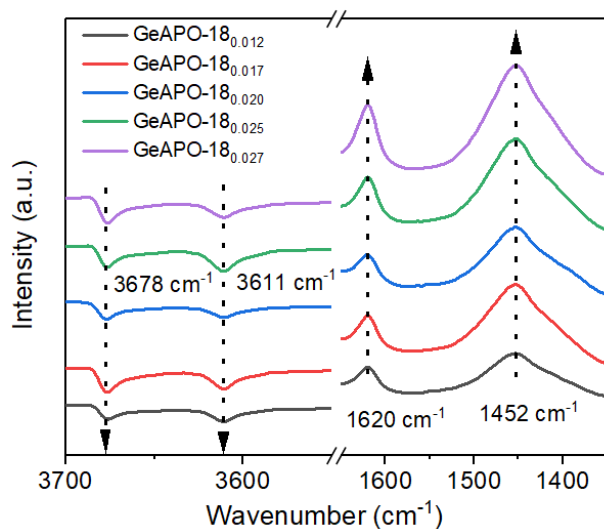
**Fig. S4. Element mapping of GeAPO-18<sub>0.025</sub>, which shows homogeneously distributed Ge species.**



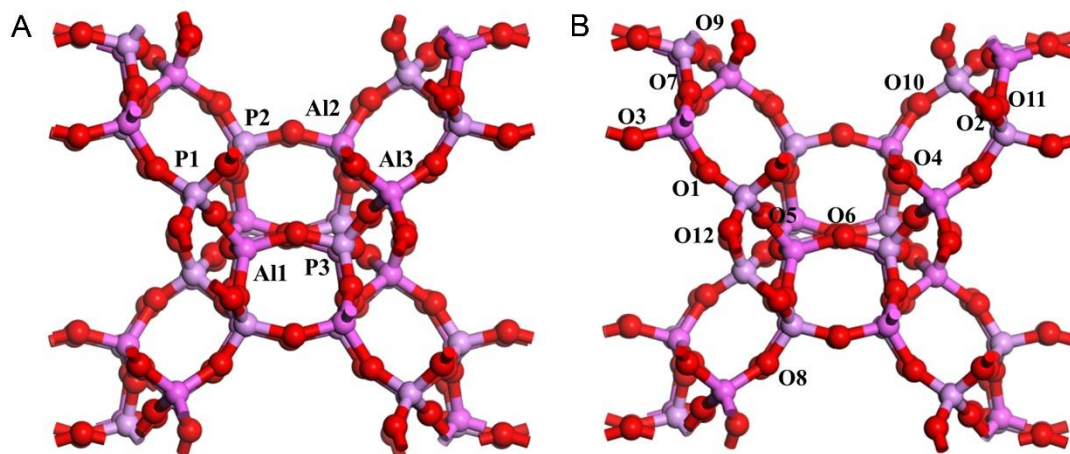
**Fig. S5. X-ray Absorption Spectra of the Ge K-edge in the R-space and k-space.** (A, D)  $\text{GeO}_2$  reference; (B, E) Fresh  $\text{GeAPO-18}_{0.025}$ ; (C, F)  $\text{GeAPO-18}_{0.025}$  in combination with  $\text{ZnCrO}_x$  after syngas reaction for 30 h. Fig. S5B shows only the first shell Ge-O at distance of 1.1 Å and no second shell corresponding to Ge-O-Ge as in  $\text{GeO}_2$  reference (fig. S5A). It confirms that the germanium species are dispersed as single sites throughout  $\text{GeAPO-18}$ . EXAFS analysis indicates that Ge is fourfold coordinated with the O atom (table S3), which is characteristic for the framework Ge, revealing the location of Ge within the framework of  $\text{GeAPO-18}$ . The coordination structure of Ge does not change even after 30 h reaction (fig. S5C), indicating a stable structure.



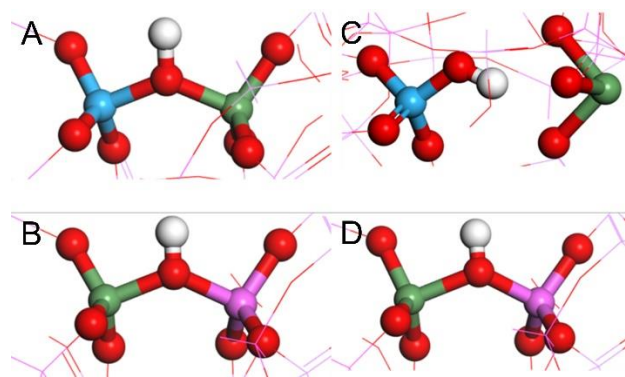
**Fig. S6. IR spectra of the hydroxyl stretching vibration of GeAPO-18<sub>a</sub> samples.** All samples exhibit a strong absorption band at 3611 cm<sup>-1</sup>. It is characteristic of the Brønsted acid sites O-H vibration associated with Ge-OH-Al. In addition, the vibration corresponding to P-OH (3678 cm<sup>-1</sup>) is also observed (16, 18).



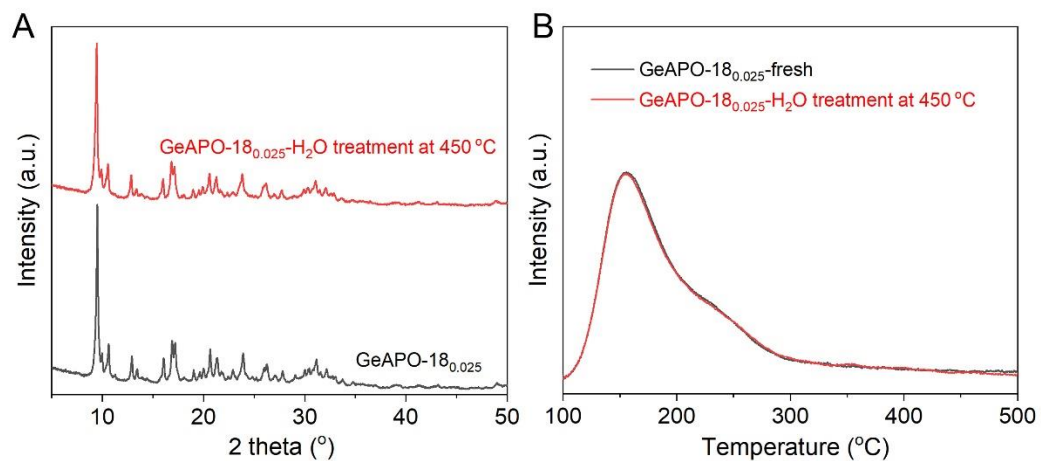
**Fig. S7. Differential IR spectra of NH<sub>3</sub>-adsorbed GeAPO-18 by referring to that of the corresponding pristine GeAPO-18.** The negative bands 3611 and 3678 cm<sup>-1</sup> in the differential spectra correspond to consumed Brønsted acid sites and P-OH sites upon NH<sub>3</sub> adsorption, respectively. The bands 1452 cm<sup>-1</sup> is attributed to the NH<sub>3</sub>-adsorbed Brønsted acid sites or P-OH, and 1620 cm<sup>-1</sup> is attributed to Lewis acid sites (16, 18). These data further validate the successful substitution of P by Ge atoms within the framework of AlPO-18, and thus generating Brønsted acid sites.



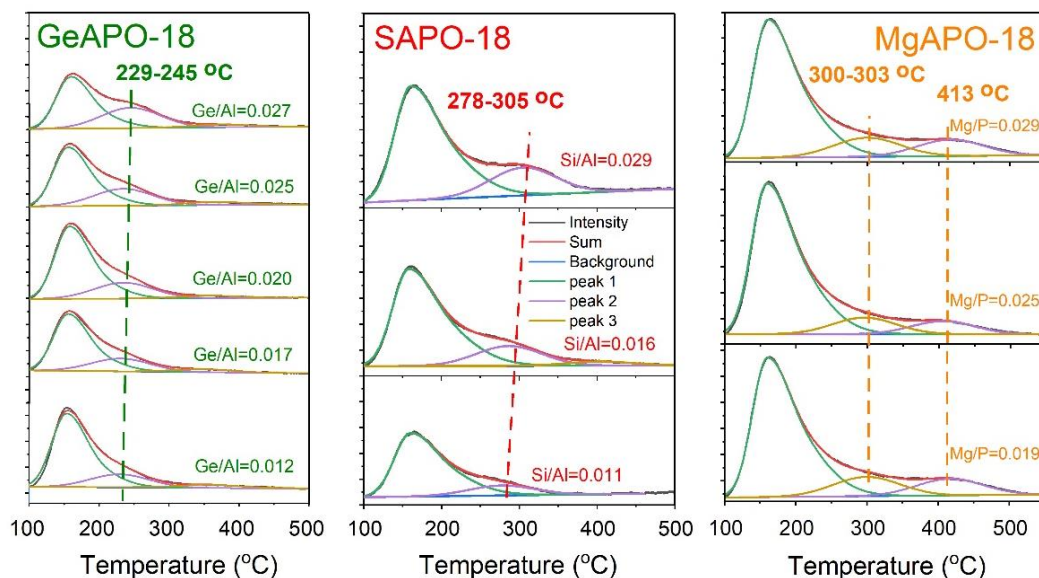
**Fig. S8. Structure scheme of AEL. (A) Al, P sites. (B) O sites with the pink, red and purple balls representing Al, O and P, respectively.**



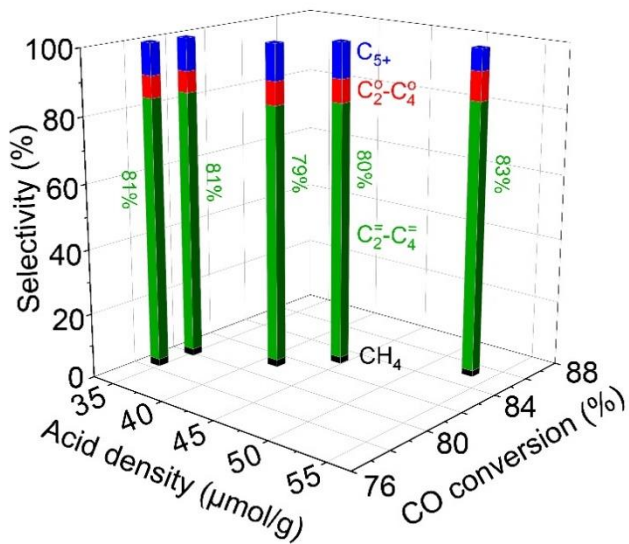
**Fig. S9. DFT calculation of GeAPO-18 structural stability.** (A) The initial structure model with Ge replacing the Al site (T1) of AEI structure (fig. S8). (B) The initial structure model with Ge replacing the P site (T1). (C) The final structure after relaxation, i.e. Ge-O bond being dissociated, indicating the unstable structure of Ge-OH-P. (D) The final structure Ge-OH-Al after relaxation, which retains the same as the initial one, demonstrating a stable structure of Ge-OH-Al. The green, pink, blue, red, and white balls represent the Ge, Al, P, O and H atoms, respectively. Therefore, Ge species most likely replace the P site in the aluminophosphate framework.



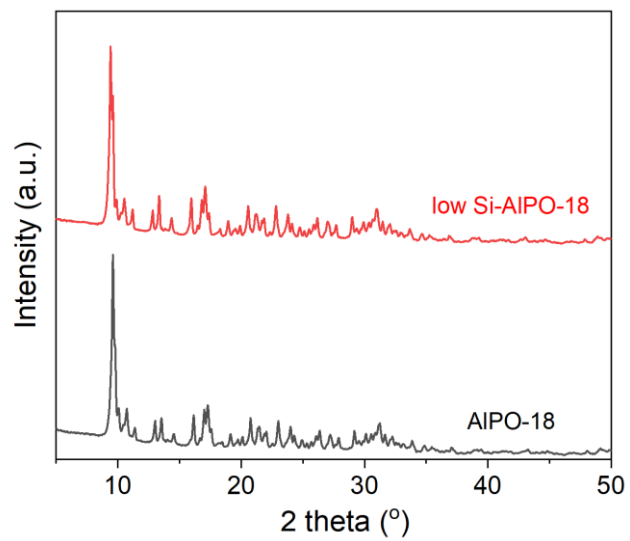
**Fig. S10. (A) XRD patterns and (B) NH<sub>3</sub>-TPD profiles for GeAPO-18<sub>0.025</sub> before and after hydrothermal treatment in flowing N<sub>2</sub> containing 10% mol H<sub>2</sub>O at 450 °C for 4 h.**



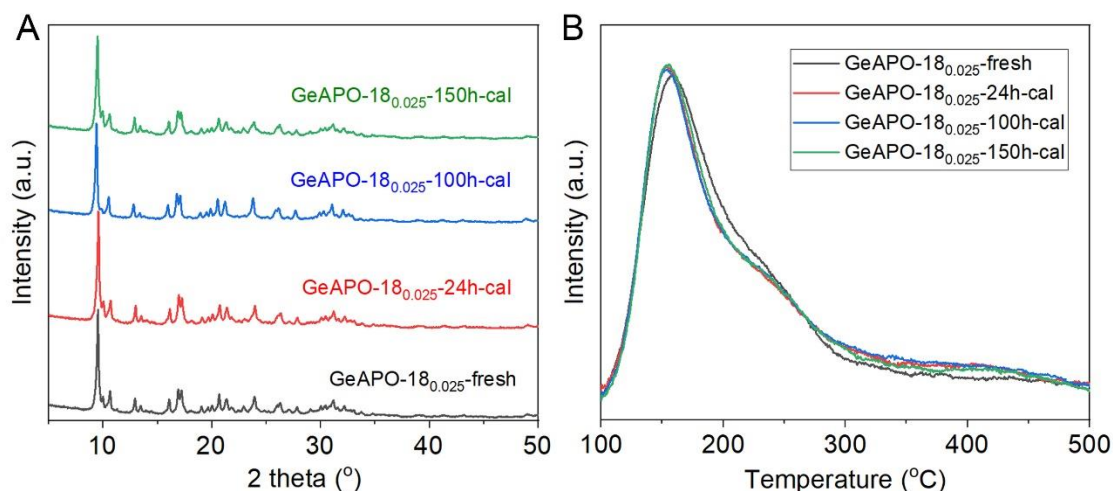
**Fig. S11.**  $\text{NH}_3$ -TPD profiles for GeAPO-18, SAPO-18 and MgAPO-18 with varying Ge/Al, Si/Al and Mg/P ratios. Deconvolution of the profiles indicates that the peak maximum being located below 200 °C is attributed to  $\text{NH}_3$  desorption from the weak acid sites while that in the range from 229-413 °C to the medium strength acid sites. Their densities can be estimated according to the integrated area and are listed in table S4. The  $\text{NH}_3$  desorption temperature reflects the acidity strength.



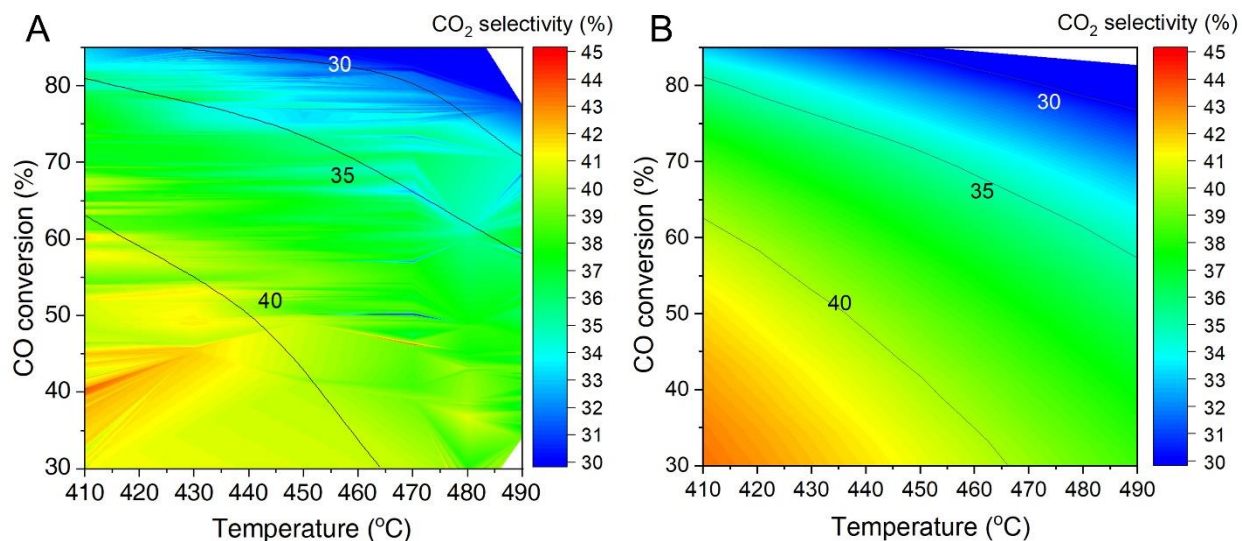
**Fig. S12. Catalytic performance as a function of the medium strength acid density of GeAPO-18.** The density of the medium strength acid sites was estimated according to the integrated desorption peaks of  $\text{NH}_3$ -TPD in fig. S11 and summarized in table S4. Reaction condition:  $\text{ZnCrO}_x/\text{GeAPO-18}$  mass ratio = 2,  $430^\circ\text{C}$ ,  $\text{H}_2/\text{CO} = 2.5$ , 6 MPa and  $1500 \text{ mL}/(\text{g}_{\text{cat}}\cdot\text{h})$ .



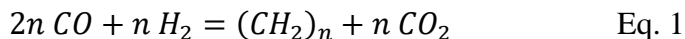
**Fig. S13. XRD patterns of AIPO-18 and low Si-AIPO-18.**



**Fig. S14. (A) XRD patterns and (B) NH<sub>3</sub>-TPD for GeAPO-18<sub>0.025</sub> before and after syngas reaction for 24, 100 and 150 h.** The crystal structure of the GeAPO-18 remains intact after 150 h reaction test. Prior to NH<sub>3</sub>-TPD, the sample was subjected to calcination in air at 600 °C to eliminate the influence from any carbon species. Fig. S14B reveals that there is slight change for the profile of the sample after 24 h reaction in comparison to the fresh sample. However, the NH<sub>3</sub>-TPD profiles are almost identical for the samples after 24, 100 and 150 h, demonstrating stable Brønsted acidity during the reaction, consistent with the stable performance in Fig. 2B. Therefore, the Ge species remain in the framework of GeAPO-18 after reaction. ICP-OES analysis of the used zeotype (table S6) indicates a negligible migration of Zn species.



**Fig. S15. Contour plots of CO<sub>2</sub> concentration as a function of temperature and CO conversion.** (A) Experimental data corresponding to Fig. 3. (B) CO<sub>2</sub> concentration at the thermodynamic equilibrium calculated using HSC 9 assuming C<sub>2</sub>H<sub>4</sub>, CO<sub>2</sub> and H<sub>2</sub>O as products under CO conversion between 30% and 90%. Reaction condition: H<sub>2</sub>/CO = 2.5, 6 MPa, temperature 410-490 °C. The two contours are very similar, suggesting that CO<sub>2</sub> selectivity is largely controlled by thermodynamics and it will decrease further with the increasing CO conversion.



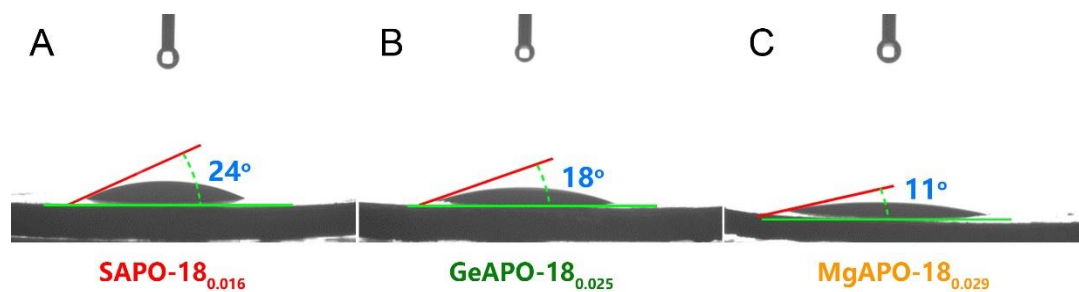


**Fig. S16. Water-droplet contact angle.** (A) SAPO-18<sub>0.016</sub> (B) GeAPO-18<sub>0.025</sub> and (C) MgAPO-18<sub>0.029</sub>. The three zeotypes all exhibit a contact angle less than 30°, indicating a similar hydrophilic property.

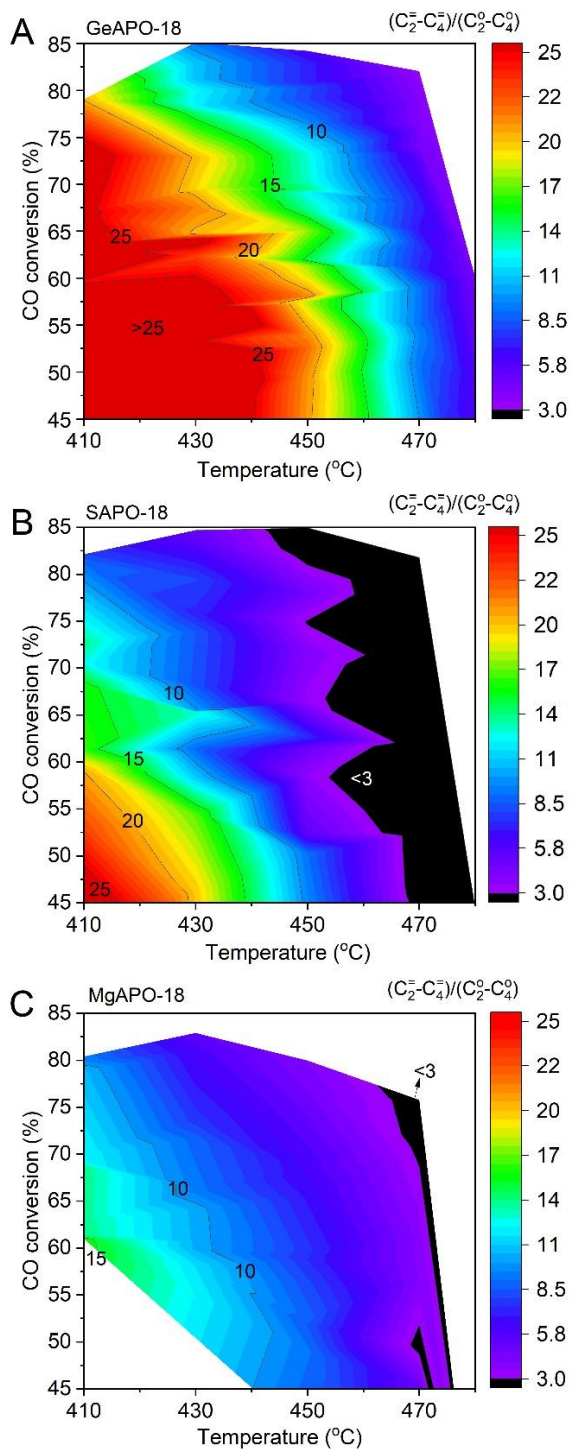


**Fig. S17. Contour plots of the ratio of light olefins to paraffins as functions of CO conversion and reaction temperature. (A) ZnCrO<sub>x</sub>-GeAPO-18; (B) ZnCrO<sub>x</sub>-SAPO-18; (C) ZnCrO<sub>x</sub>-MgAPO-18. The red-orange-yellow-green region represents  $(C_2^= - C_4^=) / (C_2^o - C_4^o) > 15$  and the black region represents  $(C_2^= - C_4^=) / (C_2^o - C_4^o) < 3$ .**

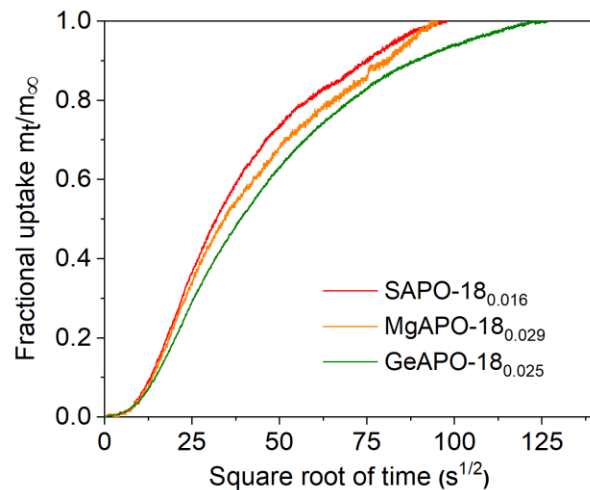


**Fig. S18. Diffusion of ethane in GeAPO-18<sub>0.025</sub>, SAPO-18<sub>0.016</sub> and MgAPO-18<sub>0.029</sub>, analyzed by IGA at 30 °C.** The diffusion coefficients of ethane were estimated to be  $2.9 \times 10^{-18} \text{ m}^2/\text{s}$  for SAPO-18<sub>0.016</sub>,  $2.3 \times 10^{-18} \text{ m}^2/\text{s}$  for MgAPO-18<sub>0.029</sub> and  $2.1 \times 10^{-18} \text{ m}^2/\text{s}$  for GeAPO-18<sub>0.025</sub>, assuming the same diffusion length (100 nm) taking the crystal size into consideration. Therefore, the diffusion efficiency of ethane was similar among the three zeotypes.

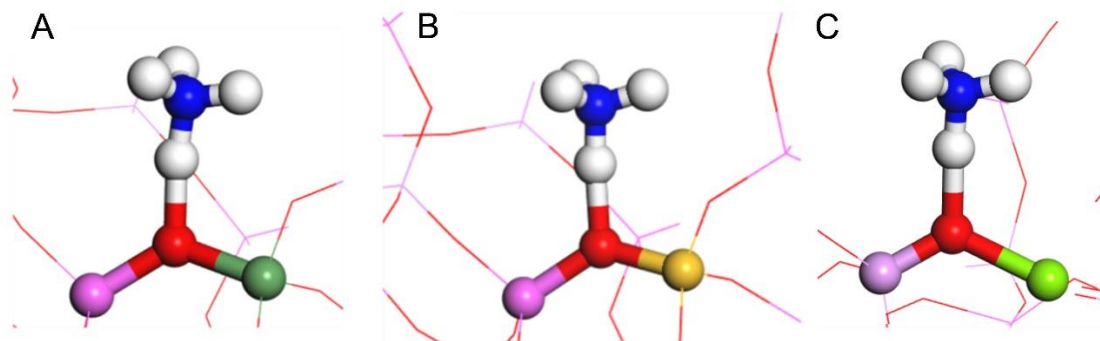


**Fig. S19.** The optimized structures of  $\text{NH}_3$  binding on the Brønsted acid sites of (A) Ge-OH-Al (T3); (B) Si-OH-Al (T3) and (C) Mg-OH-P (T1) with the olive, yellow, green, pink, red, blue and white balls representing Ge, Si, Mg, Al(P), O, N and H atoms, respectively.

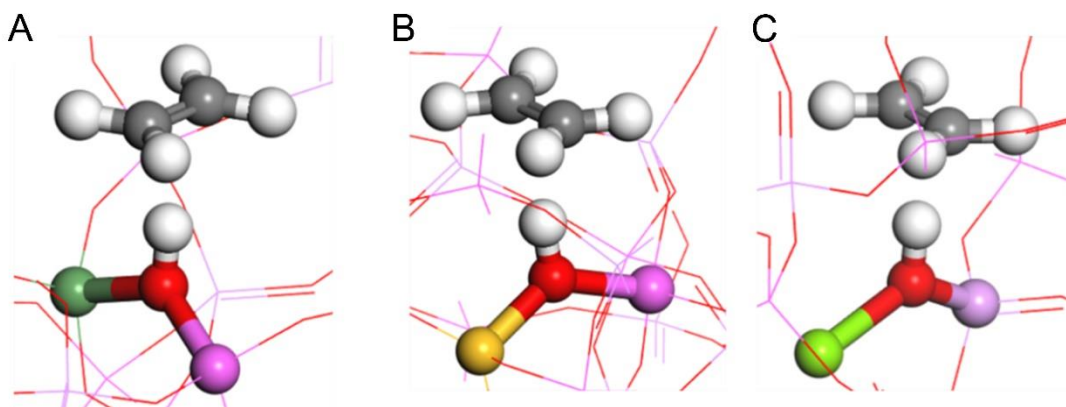


**Fig. S20.** The optimized structures of ethylene binding on the Brønsted acid sites of (A) Ge-OH-Al; (B) Si-OH-Al and (C) Mg-OH-P with the olive, yellow, green, pink, red, grey and white balls representing Ge, Si, Mg, Al(P), O, C and H atoms, respectively.

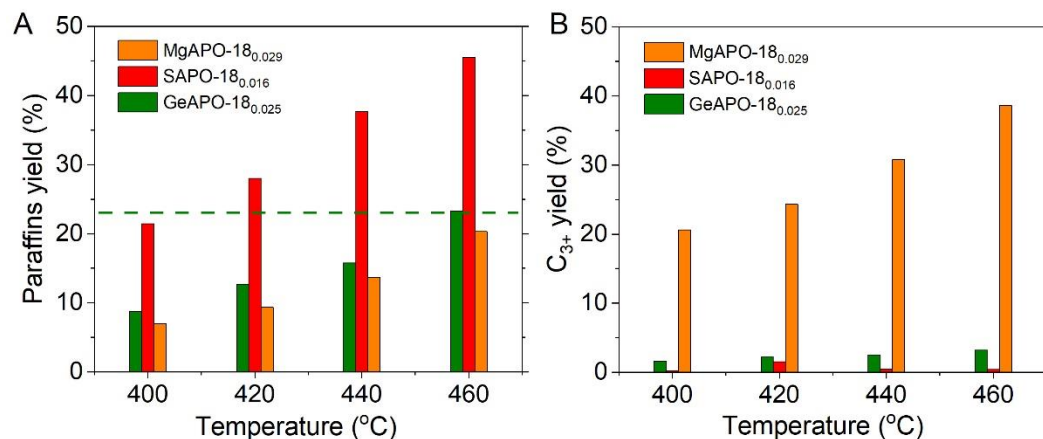


**Fig. S21. Hydrogenation and oligomerization activity during ethylene conversion in H<sub>2</sub>.** (A) Paraffins yield and (B) C<sub>3+</sub> yield. Reaction condition: 250 mg sample diluted by 200 mg quartz sands, 400 - 460 °C, 4 MPa, 200 mL/min feed composed of 1.2% C<sub>2</sub>H<sub>4</sub>, 66.6% H<sub>2</sub> and 32.2% Ar. Note that the hydrogen activity is reflected by the yield of paraffins and the oligomerization activity by the yield of hydrocarbons containing 3 and more than 3 carbon atoms.

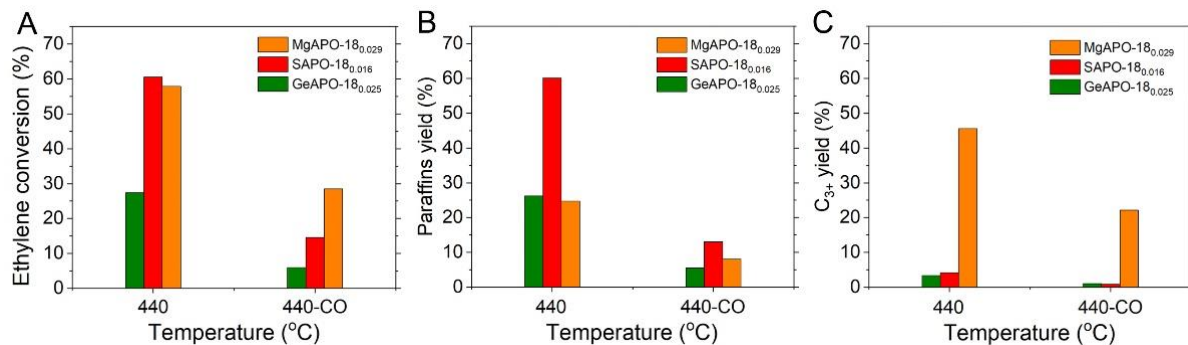


**Fig. S22. Effect of CO on the ethylene/H<sub>2</sub> model reaction.** (A) Ethylene conversion; (B) Paraffins yield and (C) C<sub>3+</sub> yield. Reaction condition: 250 mg sample diluted by 200 mg quartz sand, 440 °C, 4 MPa, 100 mL/min gas mixture composed of 1.2% C<sub>2</sub>H<sub>4</sub>-66.6% H<sub>2</sub>-32.2% Ar with/without CO (40 mL/min, 10% CO-90% Ar). The hydrogenation activity is reflected by the yield of paraffins and the oligomerization activity by the yield of hydrocarbons containing 3 and more than 3 carbon atoms.

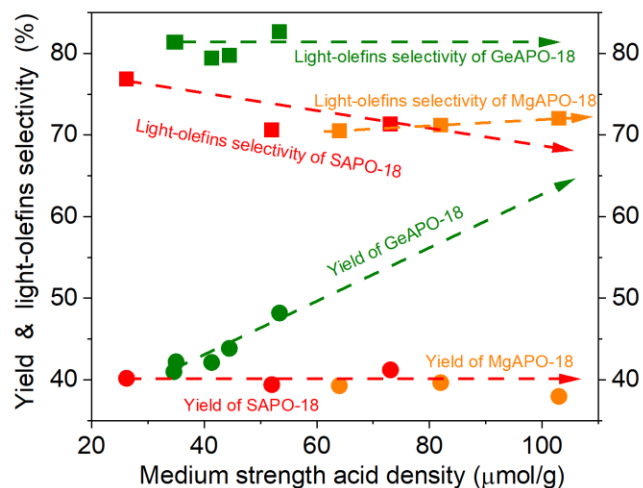


**Fig. S23. The yield and selectivity of light olefins as a function of medium strength acid density of GeAPO-18 and SAPO-18.** Reaction condition:  $H_2/CO = 2.5$ ,  $430\text{ }^\circ\text{C}$ ,  $6\text{ MPa}$ ,  $1500\text{ mL}/(\text{g}_{\text{cat}}\cdot\text{h})$ . It shows that the  $C_2=C_4$  selectivity over GeAPO-18 keeps almost unchanged (green line) whereas it decreases (red line) with the increasing density of medium strength acid sites over SAPO-18. As a result, the yield of light olefins increases almost linearly with the acid site density over GeAPO-18. The extrapolated line (dashed green line) predicts that the yield could go beyond 60% at a density of  $90\text{ }\mu\text{mol/g}$ .

**Table S1. Summary of the reported yield of light olefins in direct syngas conversion.**

Catalyst	CO conversion,%	C <sub>2</sub> =-C <sub>4</sub> = selectivity, %		C <sub>2</sub> =-C <sub>4</sub> = yield, %	Ref.
		CO <sub>2</sub> -excluded	CO <sub>2</sub> -included		
Fe/CNF <sup>a</sup>	88	52	30	26	(8)
FeMn@Si <sup>b</sup>	56	~27	~24	~14	(9)
Na-FeC <sub>x</sub> /s-S1-OH <sup>c</sup>	83	29	15	13	(10)
Mn-promoted Co <sub>2</sub> C <sup>d</sup>	32	61	32	10	(11)
CoMn-Na <sub>2</sub> S <sup>e</sup>	0.8	54	54	0.4	(12)
CoMnC/PDVB <sup>f</sup>	64	71	38	24	(13)
ZnCrO <sub>x</sub> -SAPO-34 <sup>g</sup>	17	80	47	8	(6)
ZnCrO <sub>x</sub> -SAPO-18 <sup>h</sup>	49	83	42	21	(16)
ZnCrO <sub>x</sub> -SAPO-34 <sup>i</sup>	60	75	45	27	(24)
ZnGaO <sub>x</sub> -SAPO-34 <sup>j</sup>	50	75	45	23	(21)
ZnCrO <sub>x</sub> -GeAPO-18 <sub>0.027</sub> <sup>k</sup>	85	83	57	48	This work
ZnCrO <sub>x</sub> -GeAPO-18 <sub>0.027</sub> <sup>l</sup>	70	89	57	40	This work

<sup>a</sup> H<sub>2</sub>/CO = 1, 340 °C, 2 MPa, 1500 mL/(g·h)

<sup>b</sup> H<sub>2</sub>/CO = 2, 320 °C, 2 MPa, 4000 mL/(g·h) estimated from Fig. 1B of ref. (9)

<sup>c</sup> H<sub>2</sub>/CO = 1, 260 °C, 2 MPa, 600 mL/(g·h)

<sup>d</sup> H<sub>2</sub>/CO = 2, 250 °C, 0.1 MPa, 2000 mL/(g·h)

<sup>e</sup> H<sub>2</sub>/CO = 2, 240 °C, 0.1 MPa, 27000 mL/(g·h)

<sup>f</sup> H<sub>2</sub>/CO = 2, 250 °C, 0.1 MPa, 900 mL/(g·h)

<sup>g</sup> H<sub>2</sub>/CO = 2.5, 400 °C, 2.5 MPa, 7714 mL/(g·h)

<sup>h</sup> H<sub>2</sub>/CO = 1, 390 °C, 10 MPa, 3600 mL/(g·h)

<sup>i</sup> H<sub>2</sub>/CO = 2.5, 400 °C, 4 MPa, 5000 mL/(g·h)

<sup>j</sup> H<sub>2</sub>/CO = 2.5, 400 °C, 4 MPa, 1600 mL/(g·h)

<sup>k</sup> H<sub>2</sub>/CO = 2.5, 430 °C, 6 MPa, 1500 mL/(g·h)

<sup>l</sup> H<sub>2</sub>/CO = 2.5, 430 °C, 6 MPa, 4500 mL/(g·h)

**Table S2. Elementary composition of GeAPO-18, SAPO-18 and MgAPO-18. <sup>a</sup>**

Sample	Si, Ge or Mg wt%	Al wt%	P wt%	O w%	Ge/Al, Si/Al or Mg/P ratio
GeAPO-18 <sub>0.012</sub>	0.28	23.00	24.50	52.22	0.012
GeAPO-18 <sub>0.017</sub>	0.39	23.29	24.18	52.15	0.017
GeAPO-18 <sub>0.020</sub>	0.46	23.22	24.16	52.15	0.020
GeAPO-18 <sub>0.025</sub>	0.59	23.22	24.09	52.06	0.025
GeAPO-18 <sub>0.027</sub>	0.64	23.43	23.91	52.01	0.027
SAPO-18 <sub>0.011</sub>	0.26	23.84	23.73	52.15	0.011
SAPO-18 <sub>0.016</sub>	0.39	23.60	23.81	52.20	0.016
SAPO-18 <sub>0.029</sub>	0.70	23.70	23.44	52.15	0.029
MgAPO-18 <sub>0.019</sub>	0.46	23.16	24.21	52.17	0.019
MgAPO-18 <sub>0.025</sub>	0.62	22.77	24.42	52.19	0.025
MgAPO-18 <sub>0.029</sub>	0.70	22.85	24.30	52.16	0.029
GeAPO-11 <sub>0.026</sub>	0.63	23.81	23.56	51.94	0.026
GeAPO-5 <sub>0.031</sub>	0.72	23.32	23.55	51.64	0.031
AlPO-18	0	23.25	24.47	52.28	0
low Si-AlPO-18	0.023	23.16	24.53	52.30	0.001

<sup>a</sup>: measured by XRF.

**Table S3. EXAFS fitting data.**

Sample	CN (Ge-O)	R Å	$\sigma^2$ $10^{-3}\text{Å}^2$	$E_0$ keV	R-factor %
GeAPO-18 <sub>0.025</sub>	4*	1.77±0.02	4.3±1.9	5.33±2.9	0.024
GeAPO-18 <sub>0.025</sub> -30h	4*	1.75±0.01	5.2±1.6	3.50±2.5	0.017

Ge-O path,  $S_o^2 = 0.77$ , CN = 4\* (fixed), k-range from 3 to 12.2, R-range from 1 to 2.2.

**Table S4. Acidity of GeAPO-18, SAPO-18 and MgAPO-18. <sup>a</sup>**

Sample	Weak acid density	Medium strength acid density
	$\mu\text{mol/g}$	$\mu\text{mol/g}$
GeAPO-18 <sub>0.012</sub>	161	35
GeAPO-18 <sub>0.017</sub>	103	35
GeAPO-18 <sub>0.020</sub>	157	41
GeAPO-18 <sub>0.025</sub>	129	44
GeAPO-18 <sub>0.027</sub>	113	53
SAPO-18 <sub>0.011</sub>	179	26
SAPO-18 <sub>0.016</sub>	281	52
SAPO-18 <sub>0.029</sub>	331	73
MgAPO-18 <sub>0.019</sub>	392	64
MgAPO-18 <sub>0.025</sub>	437	82
MgAPO-18 <sub>0.029</sub>	400	103

<sup>a</sup>: Estimated according to NH<sub>3</sub>-TPD in fig. S11, with the desorption peak temperature < 200 °C being attributed to the weak strength acid sites and the temperature > 200 °C to the medium strength acid sites.

**Table S5. Comparison of syngas conversion performance between AlPO-18 and GeAPO-18 in combination with ZnCrO<sub>x</sub>.<sup>a</sup>**

Zeotype samples	Si/Al or Ge/Al	CO conv., %	CO <sub>2</sub> sel., %	CH <sub>4</sub> in HCs, <sup>b</sup> %	C <sub>2</sub> <sup>=</sup> -C <sub>4</sub> <sup>=</sup> in HCs, %	C <sub>2</sub> <sup>o</sup> -C <sub>4</sub> <sup>o</sup> in HCs, %	C <sub>5+</sub> in HCs %	Light olefins yield, %
AlPO-18	0	24	41	8	63	18	11	9
Low Si AlPO-18 <sub>0.001</sub>	0.001	49	39	3	77	10	10	23
GeAPO-18 <sub>0.027</sub>	0.027	85	32	2	83	9	7	48

<sup>a</sup>Reaction condition: ZnCrO<sub>x</sub>/zeotype = 2 (mass), H<sub>2</sub>/CO = 2.5, 430 °C, 6 MPa, 1500 mL/(g<sub>cat</sub>·h).

<sup>b</sup>HCs representing "hydrocarbons".

**Table S6. Inductively coupled plasma optical emission spectrometry (ICP-OES) analysis of the Zn content of the fresh and used GeAPO-18.**

	Zn content (ppm)
Fresh GeAPO-18 <sub>0.025</sub>	4
Used GeAPO-18 <sub>0.025</sub>	52

**Table S7. Differential adsorption heat of NH<sub>3</sub> over GeAPO-18, SAPO-18 and MgAPO-18 measured by microcalorimetric method.**

	GeAPO-18 <sub>0.025</sub>	SAPO-18 <sub>0.016</sub>	MgAPO-18 <sub>0.029</sub>
Differential adsorption heat, kJ/mol	143	156	193

**Table S8. NH<sub>3</sub> binding energy over different T-sites of GeAPO-18, SAPO-18 and MgAPO-18.<sup>a</sup>**

SAPO-18		GeAPO-18		MgAPO-18	
T-site	Energy, eV	T-site	Energy, eV	T-site	Energy, eV
T1-O5	-1.39	T1-O5	-1.26	T1-O5	-1.73
T2-O3	-1.39	T2-O3	-1.25	T2-O3	-1.72
T3-O7	-1.43	T3-O7	-1.22	T3-O8	-1.69
Average	-1.40	Average	-1.24	Average	-1.71

<sup>a</sup>: see figs. S8 and S19 for the structures.

**Table S9. C<sub>2</sub>H<sub>4</sub> binding energy over different T-sites of GeAPO-18, SAPO-18 and MgAPO-18.<sup>a</sup>**

SAPO-18		GeAPO-18		MgAPO-18	
T-site	Energy, eV	T-site	Energy, eV	T-site	Energy, eV
T1-O4	-0.60	T1-O4	-0.58	T1-O5	-0.64
T1-O5	-0.60	T1-O5	-0.53	T1-O6	-0.70
T1-O10	-0.60	T1-O10	-0.58	T1-O9	-0.66
T1-O12	-0.60	T1-O12	-0.55	T1-11	-0.61
T2-O2	-0.71	T2-O2	-0.62	T2-O3	-0.65
T2-O3	-0.56	T2-O3	-0.49	T2-O4	-0.70
T2-O8	-0.76	T2-O8	-0.62	T2-O7	-0.76
T2-O11	-0.60	T2-O11	-0.54	T2-10	-0.68
T3-O1	-0.54	T3-O1	-0.51	T3-O1	-0.59
T3-O6	-0.57	T3-O6	-0.61	T3-O2	-0.71
T3-O7	-0.64	T3-O7	-0.59	T3-O8	-0.68
T3-O9	-0.58	T3-O9	-0.52	T3-12	-0.61

<sup>a</sup>: See figs. S8 and S20 for the structures.

**Table S10. Syngas conversion performance over ZnCrO<sub>x</sub>-GeAPO-18<sub>0.025re</sub> under different reaction conditions.<sup>a</sup>**

Temperature °C	GHSV mL/(g·h)	Pressure MPa	CO conversion %	CO <sub>2</sub> selectivity %	C <sub>2</sub> =-C <sub>4</sub> = in HCs %	C <sub>2</sub> =-C <sub>3</sub> = in HCs %
420	1500	6	81	36	80	55
420	1500	8	82	35	80	54
420	3000	8	73	36	82	57
430	1500	4	75	37	83	60
430	4500	4	56	40	89	68
430	1500	6	84	32	83	56
430	4500	6	71	36	84	59
430	3000	8	82	33	81	54
430	4500	8	77	35	84	57
440	4000	8	80	33	80	54

<sup>a</sup>: Reaction condition: ZnCrO<sub>x</sub>/zeotype = 2 (mass), H<sub>2</sub>/CO = 2.5.

Note that GeAPO-18<sub>0.025re</sub> is a sample of reproducing batch.

**Table S11. Syngas conversion performance over ZnCrO<sub>x</sub>-SAPO-18<sub>0.016</sub> under different reaction conditions.<sup>a</sup>**

Temperature °C	GHSV mL/(g·h)	Pressure MPa	CO conversion %	CO <sub>2</sub> selectivity %	C <sub>2</sub> =-C <sub>4</sub> = in HCs %	C <sub>2</sub> =-C <sub>3</sub> = in HCs %
420	1500	6	83	35	72	42
420	1500	8	88	32	60	29
420	3000	8	81	33	68	39
430	1500	4	70	38	65	39
430	4500	4	45	41	77	54
430	1500	6	82	32	74	44
430	4500	6	70	37	75	46
430	3000	8	84	32	72	42
430	4500	8	78	34	69	39
440	4000	8	81	33	72	43

<sup>a</sup>: Reaction condition: ZnCrO<sub>x</sub>/zeotype = 2 (mass), H<sub>2</sub>/CO = 2.5.

**Table S12. Comparison of syngas conversion performance between GeAPO-11, GeAPO-5 and GeAPO-18 in combination with ZnCrO<sub>x</sub>.<sup>a</sup>**

	Ge/Al ratio <sup>b</sup>	CO conv. %	CO <sub>2</sub> sel. %	CH <sub>4</sub> in HCs %	C <sub>2</sub> <sup>=</sup> -C <sub>4</sub> <sup>=</sup> in HCs %	C <sub>2</sub> <sup>o</sup> -C <sub>4</sub> <sup>o</sup> in HCs %	C <sub>5</sub> <sup>+</sup> in HCs %
GeAPO-11 <sub>0.026</sub>	0.026	19	44	37	8	24	30
GeAPO-5 <sub>0.031</sub>	0.031	75	38	4	30	36	30
GeAPO-18 <sub>0.027</sub>	0.027	85	32	2	83	9	7

<sup>a</sup>: Reaction condition: ZnCrO<sub>x</sub>/zeotype = 2 (mass), H<sub>2</sub>/CO = 2.5, 430 °C, 6 MPa, 1500 mL/(g<sub>cat</sub>·h).

<sup>b</sup>: Measured by XRF. The results show that the type of AlPO molecular sieves is an important factor and the AEI topology with 8-MR pores is selective for synthesis of light olefins from syngas.